Conformational Changes of gp120 in Epitopes near the CCR5 Binding Site Are Induced by CD4 and a CD4 Miniprotein Mimetic†

Wentao Zhang,‡ Gabriela Canziani,‡ Carmela Plugariu,‡ Richard Wyatt,§ Joseph Sodroski,§ Raymond Sweet,|| Peter Kwong,⊥ Wayne Hendrickson,⊥ and Irwin Chaiken*,‡

Department of Medicine, School of Medicine, University of Pennsylvania, Philadelphia, Pennsylvania 19104, Department of Cancer Immunology and AIDS, Dana Farber Cancer Institute, and Department of Pathology, Harvard Medical School, Boston, Massachusetts 02115, Department of Molecular Immunology, SmithKline Beecham, King of Prussia, Pennsylvania 19406, and Howard Hughes Medical Institute, Columbia University, New York, New York 10032

Received March 19, 1999; Revised Manuscript Received May 3, 1999

ABSTRACT: Binding of the T-cell antigen CD4 to human immunodeficiency virus type 1 (HIV-1) envelope glycoprotein gp120 has been reported to induce conformational rearrangements in the envelope complex that facilitate recognition of the CCR5 coreceptor and consequent viral entry into cells. To better understand the mechanism of virus docking and cell fusion, we developed a three-component gp120−CD4−17b optical biosensor assay to visualize the CD4-induced conformational change of gp120 as seen through envelope binding to a neutralizing human antibody, 17b, which binds to epitopes overlapping the CCR5 binding site. The 17b Fab fragment was immobilized on a dextran sensor surface, and kinetics of gp120 binding were evaluated by both global and linear transformation analyses. Adding soluble CD4 (sCD4) increased the association rate of full-length JR−FL gp120 by 25-fold. This change is consistent with greater exposure of the 17b binding epitope on gp120 when CD4 is bound and correlates with CD4-induced conformational changes in gp120 leading to higher affinity binding to coreceptor. A smaller enhancement of 17b binding by sCD4 was observed with a mutant of gp120, ΔJR−FL protein, which lacks V1 and V2 variable loops and N- and C-termini. Biosensor results for JR−FL and ΔJR−FL argue that CD4-induced conformational changes in the equilibrium state of gp120 lead both to movement of V1/V2 loops and to conformational rearrangement in the gp120 core structure and that both of these lead to greater exposure of the coreceptor-binding epitope in gp120. A 17b binding enhancement effect on JR−FL also was observed with a 32-amino acid charybdotoxin miniprotein construct that contains an epitope predicted to mimic the Phe 43/Arg 59 region of CD4 and that competes with CD4 for gp120 binding. Results with this construct argue that CD4-mimicking molecules with surrogate structural elements for the Phe 43/Arg 59 components of CD4 are sufficient to elicit a similar gp120 conformational isomerization as expressed by CD4 itself.

Human immunodeficiency virus type 1 (HIV-1)[1] infects cells, leading to acquired immunodeficiency syndrome (AIDS), by fusion of the viral membrane with the target cell membrane (*1*, *2*). The fusion process is mediated by virus envelope glycoprotein gp120 and can be triggered by the interaction of gp120 with the T-cell antigen receptor CD4 glycoprotein (*3*−*5*). CD4, a primary receptor for gp120 (*6*−*8*), induces conformational changes in gp120 that are postulated to promote subsequent steps in the fusion process, such as coreceptor binding and dissociation of gp120 from gp41 (*9*, *10*). Recently, several seven-transmembrane chemokine receptors, mainly CCR5 and CXCR4, have been identified as obligate coreceptors for virus cell entry (*11*−*16*). Blocking the binding of CD4 with gp120, and more specifically, preventing the CD4-induced conformational isomerization that promotes coreceptor binding and viral cell fusion, could have potential therapeutic value for the treatment of HIV infection and AIDS. Such a therapeutic approach would be aided greatly by increased definition of the molecular mechanism of the conformational isomerization in the CD4−gp120−CCR5 binding process.

Conformational isomerization of gp120 can be related to the structure of this molecule. The virus envelope glycoprotein gp120 contains five conserved regions (C1−C5) and

† This work was supported by National Institutes of Health 1 PO1 GM 56550-01, Structure-Based CD4-gp120 Antagonism (IMC P.I.). This work was also supported by a Center for AIDS research grant (AI28691), and by the G. Harold and Leila Mathers Foundation, the Friends 10, Douglas and Judith Knapp, and the late William F. McCarty-Cooper.

* To whom correspondence should be addressed: Tel 215-573-9678; Fax 215-349-5572; Email *chaiken@mail.med.upenn.edu*. Mailing address: 913 Stellar-Chance Labs, 422 Curie Blvd., Philadelphia, PA 19104.

‡ University of Pennsylvania.

§ Dana Farber Cancer Institute and Harvard Medical School.

|| SmithKline Beecham.

⊥ Columbia University.

[1] Abbreviations: AIDS, acquired immunodeficiency syndrome; CD4BS, CD4 binding-site epitopes; CD4i, CD4-induced epitopes; DMF, *N*,*N*-dimethylformamide; DTT, dithiothreitol; EDC, 1-ethyl-3-[3-(dimethylamino)propyl]carbodiimide; ELISA, enzyme-linked immunosorbent assay; Env, envelope protein; Fmoc, 9-fluorenylmethoxycarbonyl; HIV-1, human immunodeficiency virus type 1; HOAT, 1-hydroxy-7-azabenzotriazole; HPLC, high-performance liquid chromatography; M-tropic, macrophage tropic; NHS, *N*-hydroxysuccinimide; PBS, phosphate-buffered saline; PDB, protein data bank; sCD4, soluble CD4; SPR, surface plasmon resonance; TFA, trifluoroacetic acid.

10.1021/bi990654o CCC: $18.00
Published on Web 07/02/1999

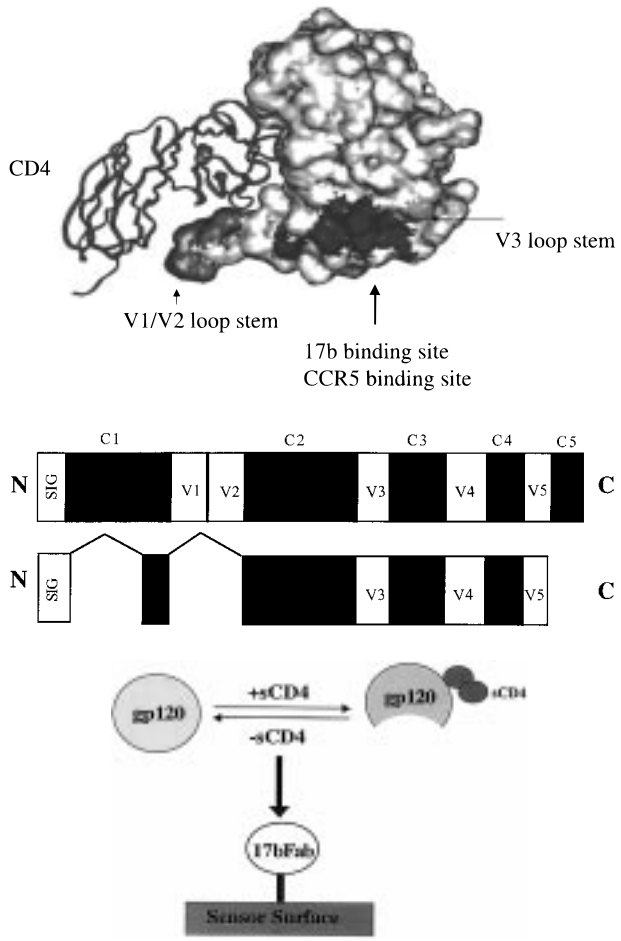

FIGURE 1: (Upper panel) Structural view of receptor binding sites on gp120 from the crystal structure of the ternary complex of core HIV-1 gp120 complexed to CD4 fragment D1D2 and the 17b Fab (*20*). The 17b Fab is not showing in the figure. (Center panel) Schematic representation of envelope proteins. Full-length JR−FL is shown in the upper figure. Conserved regions are in black and variable regions are in white. ΔJR−FL is shown in the lower diagram. The C1, V1/V2, and C5 deletions correspond to Δ89, Δ128−194, and Δ492, respectively. SIG, signal peptide; N,N-terminus; C, C-terminus. (Lower panel) Schematic representation of gp120−17b Fab−sCD4 three-component biosensor assay configuration.

five variable regions (V1−V5), identified by comparison of the primary amino acids sequences of gp120 proteins derived from different HIV-1 isolates (*17*−*19*). The conserved regions form a core structure important for the interaction with the receptors and the gp41 ectodomain (*20*−*22*). The variable regions are more hydrophilic, with V1−V4 regions forming surface-exposed looplike structures with disulfide bonds at their bases (*23*). Although the structure of the ligand-free gp120 is unknown, clues to the conformational isomerization of gp120 have been inferred from the structure of the ternary complex of core HIV-1 gp120 complexed to CD4 and the 17b Fab (Figure 1, upper panel) (*21*). Core gp120 comprises of two domains and a "bridging sheet" minidomain. Sequences that are variable (V1−V5) between different gp120 isolates form loop extensions that emanate from this central core. CD4 binds to both domains and on one face of the bridging sheet. The other face of the bridging sheet and portions of the V3 loop form the binding site for the chemokine coreceptors. Extensive mutational and antibody-mapping studies have defined the epitopes for the two most common classes of broadly neutralizing antibodies. These epitopes, the CD4 binding-site epitopes (CD4BS) and the CD4-induced epitopes (CD4i), appear to correspond to these two receptor binding surfaces (*19, 20, 24*−*29*). The CD4-induced epitopes are near the V3 loop, consist mainly of the conserved stem of V1/V2 stem-loop and of the C4 region, and are probably masked by the flanking V2 and V3 loops as indicated by mutagenic analysis (*19, 30*). These CD4i epitopes are also recognized by the human monoclonal antibody 17b, which is a member of the CD4i class of antibodies. It has been suggested that CD4 binding induces gp120 conformational rearrangements (*9, 10, 31*−*37*), one of which involves repositioning the V1/V2 loops, therefore exposing the CD4i epitopes as judged by the higher 17b binding affinity in the presence of sCD4 in immunoprecipitation and ELISA assays (*9, 10, 30, 38*). The CD4i epitopes recognized by 17b can be directly visualized in the X-ray crystal structure of the [17b Fab]−[gp120]−[CD4 fragment D1D2] ternary complex (*21*).

The presence of sCD4 also has been shown to increase dramatically the affinity of the env gp120 of macrophage-tropic (M-tropic) HIV-1 for coreceptor CCR5 (*39*). Furthermore, several observations argue for the proximity of the 17b epitope (CD4i) and the CCR5 binding site (*19, 30, 40*). These include (a) the ability of 17b to block the interaction of soluble CD4−gp120 complex with CCR5 (*29, 39*) and (b) the observation that a highly conserved gp120 structure located near or within the CD4i epitopes is critical for CCR5 binding (*26*). Hence, 17b can be used as a reporter to detect molecular events that occur at the CCR5-binding site in virus−cell docking and fusion. Use of 17b as a reportor circumvents limitations in biophysical characterization of interactions of the chemokine receptors, since the latter are integral seven-transmembrane segment molecules not easily solubilized for such characterization.

In the study reported here, we have developed a surface plasmon resonance (SPR) optical biosensor assay to measure the real-time kinetics in the CD4−gp120−17b Fab three-way complex. The binding kinetics of the 17b Fab against recombinant JR−FL gp120 protein in the presence and absence of sCD4 were examined. A modified gp120 glycoprotein, ΔJR−FL, in which the V1 and V2 variable loops as well as conserved regions C1 and C5 are deleted (Figure 1, center), also was tested in the CD4−gp120−17b Fab three-way complex biosensor assay. The structure of this mutant is closely related to the gp120 core protein in the trimolecular complex crystal structure (*21*), except that the V3 loop is intact in ΔJR−FL protein and preserves the binding sites to CD4 and antibodies against CD4BS and CD4i epitopes despite the deletions (*22, 30, 41*). The comparative binding kinetics of ΔJR−FL protein versus full-length JR−FL protein to 17b Fab in the presence and absence of sCD4 provide insights into the involvement of the V1/V2 loops and the contributions of other structural elements in conformational isomerization of CD4i epitopes and CCR5 binding site upon CD4 binding. The biosensor-based kinetics assay also was used to identify a charybdotoxin-based CD4-mimicking molecule (TXM1) that induces a conformational isomerization at the 17b binding site similar to that observed with sCD4. TXM1 contains a Phe27 side chain and Gly1 α-amino group, which resemble the Phe43/Arg59 side chain cluster in CD4 (Figure 8) that has been determined by

mutagenic and structural analysis to be key for gp120 recognition.

EXPERIMENTAL PROCEDURES

Protein Production. The human monoclonal antibody 17b, derived from an HIV-infected individual (*38*), was purified by protein A affinity chromatography. Fab fragments were produced by papain digestion of monoclonal antibodies. Briefly, the antibody was reduced in a solution containing 100 mM DTT, 100 mM NaCl, and 50 mM Tris, pH 8.0, for 1 h at 37 °C. The reacted sample was dialyzed at 4 °C, first in phosphate-buffered saline (PBS) to reduce the DTT concentration to ~1 mM, then in alkylating solution (PBS titrated to pH 7.5 with 2 mM iodoacetamide, 48 h), and finally in PBS without iodoacetamide. The reduced and alkylated antibody was concentrated to at least 2 mg/mL and digested with papain by a commercial protocol (Pierce). Gel-filtration chromagraphy on a Superdex S-200 column (Pharmacia, FPLC) was carried out to ensure oligomeric homogeneity.

Recombinant wild-type gp120 and ΔC1/ΔV1/V2/ΔC5 (Δ82/Δ128−194/Δ492; HXBc2 numbering) were derived from the JR−FL strain and were produced from stable transfected *Drosophila* Schneider 2 (S2) cell lines under the control of the metallothionein promoter as previously described (*42*). The latter of the above proteins is referred to herein as ΔJR−FL protein. Recombinant-expressed proteins were purified by passage of gp120-containing medium over an F105 Mab (anti-gp120) affinity column. After extensive washing, proteins were eluted with 100 mM glycine hydrochloride, pH 2.8, and immediately neutralized with 1 M Tris base. After spin concentration with Centriprep 30 spin filters (Amicon), recombinant proteins were stored at −20 °C in glycine hydrochloride−Tris buffer, pH 7.4, containing protease inhibitors. Soluble CD4 (sCD4) was obtained as previously described (*43*, *44*).

Optical Biosensor Binding Assays. Interaction analyses were performed with a BIA2000 optical biosensor (Biacore Inc.) with simultaneous monitoring of four flow cells. Immobilization of ligands (17b Fab and sCD4) to CM5 sensor chips was performed following the standard amine coupling procedure according to the manufacturer's specification. Briefly, carboxyl groups on the sensor chip surface were activated by injection of 35 μL of a solution containing 0.2 M EDC and 0.05 M NHS at a flow rate of 5 μL/min. Next, a protein ligand at a concentration of ~50 ng/mL in 10 mM NaOAc buffer, pH 4.5, was flowed over the chip surface at 25 °C at a flow rate of 20 μL/min until the desired level of response units of reacted protein was reached. Then, after unreacted protein was washed out, excess active ester groups on the sensor surface were capped by the injection of 35 μL of 1 M ethanolamine, pH 8.0, at a flow rate of 5 μL/min. A reference surface that was used as background to correct instrument and buffer artifacts was generated at the same time under the same conditions with omission of protein ligand.

Binding experiments were performed at 25 °C in PBS buffer, pH 7.4, with 0.005% Tween 20. Unless otherwise specified, PBS contains 10 mM phosphate and 150 mM NaCl. Association was measured by passing analyte solutions over the chip surface at a flow rate of 30, 40, or 60 μL/min for 2−4 min. The direct binding of JR−FL gp120 protein and ΔJR−FL protein to sCD4 was measured by using immobilized sCD4. The concentration range for gp120 analytes was 19.5−250 nM. When mixing with sCD4, the concentrations of gp120 were from 2.5 to 125 nM, and the concentrations of sCD4 were kept at a 15-fold and 25-fold excess over the concentration range of JR−FL gp120 protein and ΔJR−FL protein, respectively. Excess sCD4 optimized the formation of CD4−gp120 complex in solution. The gp120s and sCD4 were premixed at room temperature for at least 1 h before injection. To test the effect of peptide mimetics (TXM1 and TXM0, see below) on the 17b binding of JR−FL gp120, the molar ratios of gp120 to TXM1 and TMX0 were 1:50. In the competition assay, sCD4 was immobilized on the surface with 150 RU surface density and the molar ratio of gp120 to TXM1 was 1:20. Dissociation of bound analytes was monitored while the surface was washed with buffer for 2−4 min. Remaining analytes were removed in the surface regeneration step with a 25−30 s injection of 10 mM HCl at a flow rate of 100 μL/min.

Peptide Synthesis. The charybdotoxin derivative, TXM1, was produced on an automated PerSeptive peptide synthesizer (Model 9600) using Fmoc to protect the α-amino function and HOAT as coupling reagent (*45*−*47* and references therein). The TXM1 peptide sequence is NH_2-GCTTSKECWSVCQRLHNTSRGGCQG**SF**CTCGP-OH. A control peptide, TXM0, was synthesized in the same way with residues 26 and 27 reversed, namely, NH_2-GCTTSKECWSVCQRLHNTSRGGCQG**FS**CTCGP-OH. For these syntheses, Fmoc-Pro-Cl-trityl resin (0.57 mmol/g) was purchased from Anaspec. All side-chain-protected Fmoc amino acids—Arg(Pmc), Asn(Trt), Cys(Trt), Gln(Trt), Glu(OtBu), Gly, His(Trt), Leu, Lys(Boc), Phe, Ser(tBu), Thr(rBu), Trp(Boc), and Val—were purchased from Advanced Chemtech. The α-amino protecting group, Fmoc, was removed by 30% piperidine in DMF/toluene (1:1) solution. All residues were coupled in DMF.

After chain assembly, the peptide was freed from the resin and side-chain-deprotected simultaneously by TFA cleavage (*46*). Briefly, the peptide−resin was placed in a dry flask and was cooled in an ice-bath. Then, cold cleavage mixture, which contains 81.5% TFA, 5% phenol, 5% water, 2.5% ethanedithiol, 5% thioanisole, and 1% triisopropylsilane, was added to the peptide−resin (25 mL/g of resin). Then, the flask was removed from the ice-bath and the reaction was allowed to proceed at room temperature for 1.5 h. The cleavage reaction was stopped by vacuum filtration to separate the peptide solution from the resin support. The peptide solution was concentrated by rotary evaporation to remove most of the TFA. Cold ethyl ether was added to the concentrated mixture (about 10 times the volume of the peptide mixture) to precipitate the peptide. The crude precipitated peptide was collected by vacuum filtration.

Disulfide bonds were formed directly on the crude product by oxidation in a pH 7.8 0.1 M Tris-HCl buffer containing 0.2 M NaCl, 5 mM reduced glutathione, and 0.5 mM oxidized glutathione (*48*) at room temperature. The oxidation reaction was terminated after 4 h by lowering the pH to ~3 by 20% TFA. The reaction mixture was concentrated and desalted in an Amicon stirred cell with 1000 molecular weight cutoff membrane under nitrogen pressure.

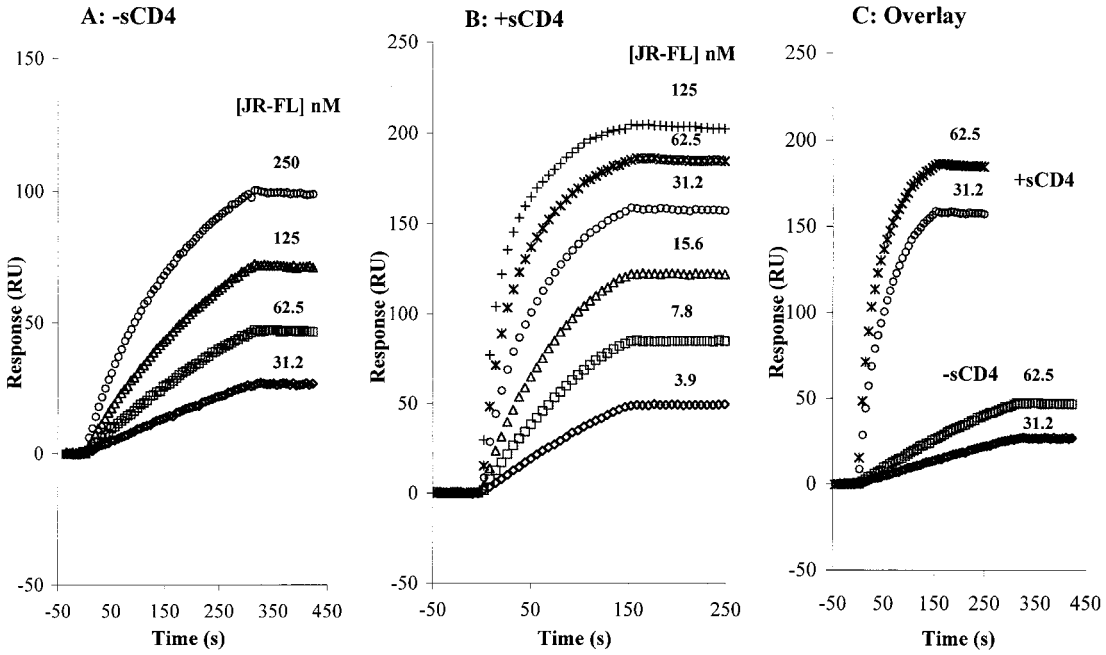

FIGURE 2: Sensorgram overlays for JR−FL binding to immobilized 17b Fab surface. Surface density, 620 RU: buffer, 10 mM phosphate, pH 7.4, 150 mM NaCl, and 0.005% Tween. JR−FL gp120 protein concentrations are shown at the right of each sensorgram. (A) In the absence of sCD4; flow rate 30 μL/min. (B) In the presence of sCD4; the sCD4 concentration in each mixture is 15 times that of each JR−FL concentration; flow rate 60 μL/min. (C) Direct sensorgram overlay comparison for JR−FL at 31.2 and 62.5 nM with or without sCD4. Note: a part of the visual difference here is due to the increase of mass (from 100 kDa for JR−FL alone to 140 kDa for the JR−FL/sCD4 complex). Nonetheless, this mass shift clearly does not account for the major changes in sensorgrams, for +sCD4, which shows much faster on rate than when sCD4 is absent.

Oxidized peptide was purified by reverse-phase HPLC on a Vydac C18 column with a linear acetonitrile gradient (10−22% buffer B in 45 min; buffer A, 0.1% TFA/5% CH_3CN; buffer B, 0.1% TFA/90% CH_3CN). The purified fraction was lyophilized to dryness and its structure was confirmed by mass spectrometry analysis in the mass spectrometry analysis core facility of the Wistar Institute.The observed mass for TXM1 was $MH^+ = 3390.11$, compared to a calculated mass of $MH^+ = 3388.85$. For TXM0, MH^+ was 3388.52 (calculated $MH^+ = 3388.85$).

RESULTS

Structural Basis for Three-Component Binding Assay. The crystallographic structure of the D1D2 CD4−gp120 core−17b Fab complex (*21*) and mutagenesis experiments (*20, 26*) confirm that the CCR5 binding site in HIV-1 env is highly conserved, involves the bridging sheet and V3 loop, and is near or within the CD4i epitope that is directly recognized by 17b antibody (Figure 1, upper panel). On the basis of this lead information, we configured an optical biosensor assay (Figure 1, lower panel) in which 17b Fab was attached to the sensor surface and used as a CCR5 surrogate to evaluate CD4-induced conformational changes in gp120 (both JR−FL and ΔJR−FL proteins, Figure 1, center panel) that affect the coreceptor binding site. The CD4-induced conformational rearrangements in gp120 and their effect on CCR5 binding were visualized by comparing the binding kinetics of gp120 proteins to immobilized 17b Fab in the absence vs presence of sCD4. The CD4-mimicking kinetic effects of a charybdotoxin miniprotein construct, TXM1, also were revealed by this assay.

Binding of Full-Length JR−FL gp120 Glycoprotein to Immobilized 17b Fab in the Absence and Presence of sCD4. To examine the effect of sCD4 on the binding kinetics of JR−FL gp120 protein to the CD4i epitope-neutralizing antibody 17b, 17b Fab was immobilized to the sensor chip surface. Three surface densities of 17b Fab, namely 150, 620, and 1670 RU, were generated by direct immobilization through amine coupling. The flow rates were 30 and 60 μL/min in the absence and presence of sCD4, respectively. Different surface densities and flow rates allowed us to eliminate mass transport as a limiting factor in observed binding kinetics and to obtain optimized experimental conditions. The sensorgrams of JR−FL gp120 protein binding to 17b Fab (620 RU surface) in the absence and presence of sCD4 are shown in Figure 2, panels A and B, respectively. Signal from the reference flow cell (FC1) was subtracted to correct for bulk effect and nonspecific binding to the surface. The interaction of 17b Fab with JR−FL gp120 protein was measured over a concentration range of JR−FL protein of 31.2−250 nM in the absence of sCD4 and of 3.9−125 nM in the presence of sCD4. For the latter, the concentration of sCD4 was kept at 15 times that of JR−FL gp120 protein. A comparison of sensorgrams obtained at identical JR−FL concentrations with and without added sCD4 is shown in Figure 2C.

The responses from the low, medium, and high surface densities at the same gp120 concentration are close to identical as judged by sensorgram overlay after normalization for maximum responses. One such set of data is shown in Figure 3. The overlap of normalized sensorgrams at varying ligand densities indicates that, under the experimental condition used, these binding reactions are not influenced by mass transport. The negligible influence of mass transport also was confirmed by global analysis, in which similar fits were found when comparing the kinetic constants

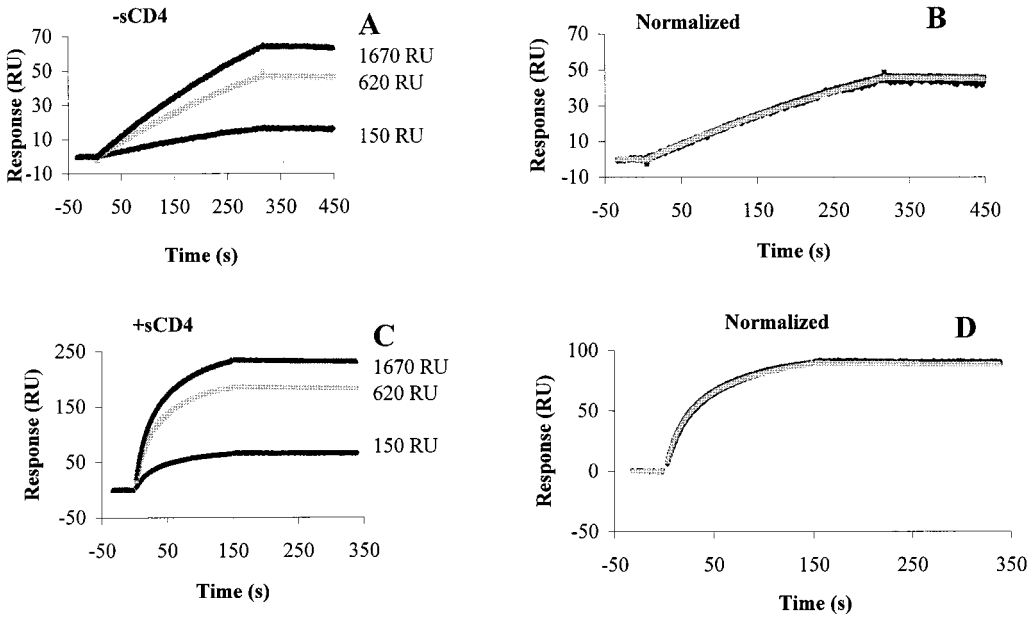

FIGURE 3: Analysis for mass transport in biosensor data. The figure shows sensorgrams of 62.5 nM JR−FL gp120 protein binding to immobilized antibody 17b Fab in the absence (A,B) and presence (C,D) of sCD4. Panels A and C show original data from three surfaces; panels B and D show data normalized for maximum level of binding signal.

obtained with a simple 1:1 binding model vs a 1:1 binding model with mass transport, and by simulation (data not shown).

As observed in the results in Figure 2, rates of association of JR−FL gp120 protein with 17b Fab are greater in the presence than in the absence of sCD4 at comparable JR−FL gp120 protein concentrations. Sensorgram data were analyzed by both linear transformation (plots II−IV in Figure 4, panels A and B) and global integration (plot I in Figure 4, panels A and B). In the absence of sCD4, the one-to-one binding model fits well with all of the data, as shown in Figure 4A. The χ^2 values (a standard statistical measure of the closeness of the fit; values below 10 are acceptable) for the global fits (Figure 4A, plot I) were all below 2. In the presence of sCD4, the one-to-one binding model fits well with the data at four low concentrations, 3.9−31.2 nM. The χ^2 values were all below 1 (Figure 4B, plot I). However, deviation from a 1:1 binding model becomes apparent at higher concentrations and indeed is suggested by the linear transformation analysis results at 31.2 nM shown in Figure 4B, plot II. The conformational change model was not employed in the data analysis when sCD4 was present, since the change in conformation expected to occur upon CD4 binding to JR−FL occurs upon mixing of these two components and before addition of the mixture to 17b Fab immobilized on the sensor surface. The kinetic constants obtained from one-to-one binding model analysis are listed in Table 1. As shown, the on-rate constant is increased sharply, 22−30-fold, for JR−FL gp120 protein−17b binding in the presence vs absence of sCD4.

As a negative control, solutions of sCD4 alone at the same concentrations as in the gp120−sCD4 mixture were tested for nonspecific binding to the same 17b Fab sensor surfaces. No binding between sCD4 and 17b Fab was detected (data not shown).

Binding of a Deleted gp120, ΔJR−FL Protein, to Immobilized 17b Fab in the Absence and Presence of sCD4. Compared with wild-type gp120, the ΔJR−FL protein lacks the N- and C-termini and the V1/V2 variable loops. Binding of ΔJR−FL protein to 17b Fab in the absence vs presence of sCD4 was monitored by using the same immobilized 17b Fab surfaces as used above for full-length JR−FL protein. Sensorgrams for the 620 RU surface are shown in Figure 5. In the presence of sCD4, the concentration of sCD4 is 25 times that of ΔJR−FL protein. Data were analyzed as with the full-length JR−FL protein as shown in Figure 6. No influence of mass transport was observed. Deviation from the 1:1 binding model was also observed at higher concentrations of ΔJR−FL protein when sCD4 was present. Linear transformation and global analyses with fit to a 1:1 binding model led to the kinetic constants for ΔJR−FL given in Table 1. When sCD4 is present, the on rate of ΔJR−FL protein to 17b Fab is increased by about 16-fold. This indicates that, as with intact JR−FL protein, ΔJR−FL protein binds 17b with a faster on rate in the presence of CD4.

Comparing JR−FL protein with ΔJR−FL protein, the on rate of ΔJR−FL protein to 17b Fab is about 5 times greater than that of JR−FL protein in the absence of sCD4. The off rates are very similar. This is consistent with the notion that the 17b epitope (CD4i) is masked by the V1/V2 loops in native gp120 molecule, whereas in ΔJR−FL protein the 17b epitope (CD4i) is more exposed since the V1/V2 loops are deleted. However, N- and C-terminal deletions in ΔJR−FL protein also could influence the binding affinity. In the presence of sCD4, the apparent equilibrium dissociation constants of ΔJR−FL and JR−FL protein to immobilized 17b Fab are very similar. K_d values were 0.041 nM and 0.1 nM, respectively. However, the kinetic analysis shows that, in the presence of sCD4, ΔJR−FL protein has a faster on rate (about 3-fold) than that for JR−FL protein (Table 1).

Binding of JR−FL and ΔJR−FL to Immobilized sCD4. Two sensor surfaces with immobilized sCD4 were created through amine coupling. The surface densities were 200 and 400 RU. The concentration ranges for JR−FL and ΔJR−

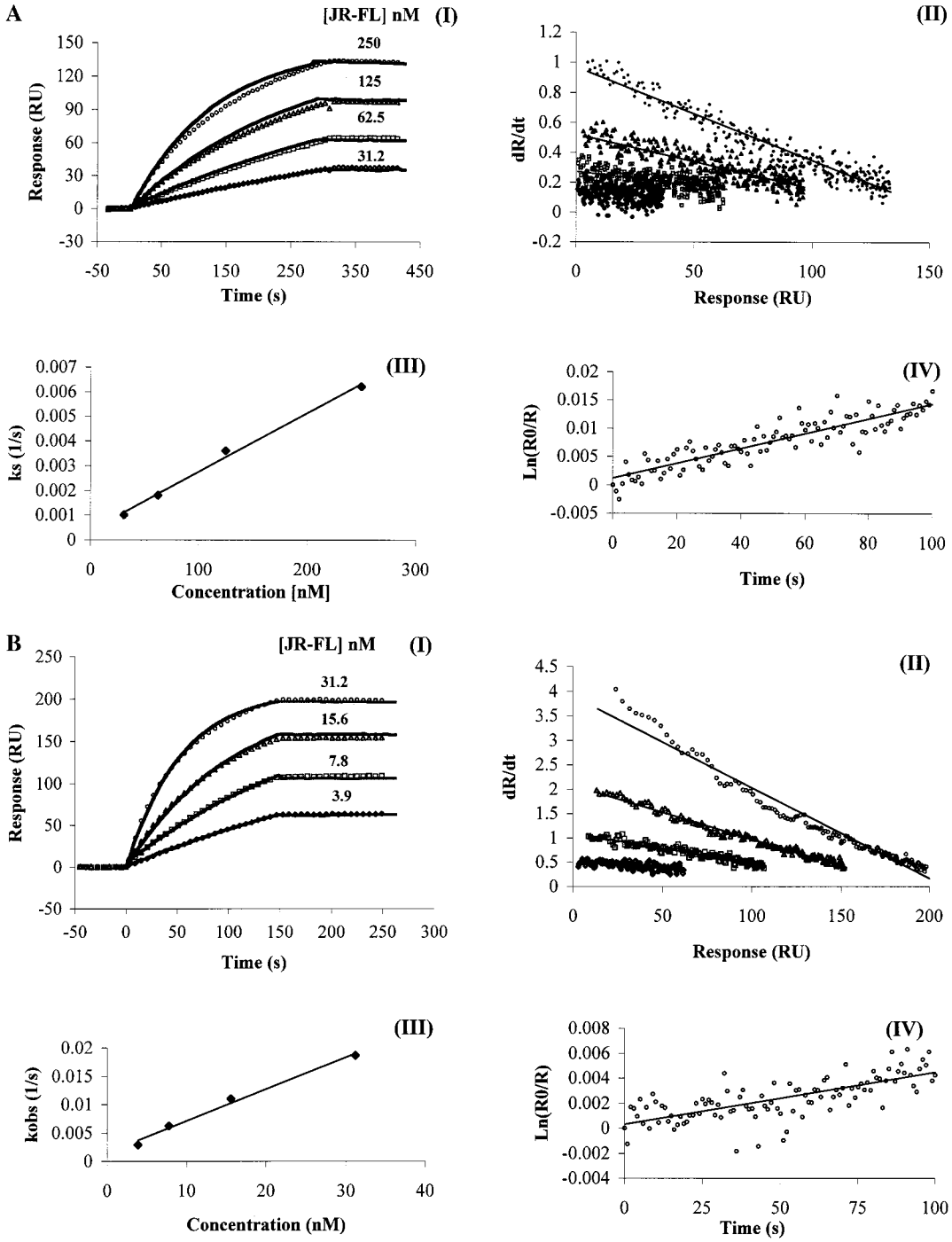

FIGURE 4: (A) Curve-fitting analysis of JR−FL gp120 protein binding to immobilized 17b (1670 RU) Fab in the absence of sCD4. (I) Global analysis: the symbols are the experimental data, the lines are the best fit to a 1:1 binding model. (II−IV) Linear transformation analyses: (II) dR/dt vs R plot; (III) k_{obs} vs concentration plot, where the slope of the line is k_{on}; (IV) ln (R_0/R) vs time plot of the 250 nM curve in plot I, where R_0 is the starting point of dissociation and the slope of the line gives k_{off}. (B) Curve-fitting analysis of JR−FL gp120 protein binding to immobilized 17b (1670 RU) Fab in the presence of sCD4. Plots I−III are as in panel A. In plot IV, the ln (R_0/R) vs time plot is for the 31.2 nM curve in plot I, where R_0 is the starting point of dissociation and the slope of the line gives k_{off}.

FL proteins were from 15.6 to 125 nM and from 9.8 to 78 nM, respectively. The overlaid sensorgrams for the 200 RU surface are shown in Figure 7. All data could be fit to a 1:1 binding model by linearization and global analyses. This correspondence indicates that there is no significant mass transport contribution in binding reactions for either surface. The χ^2 values were all below 2. The kinetic constants obtained are listed in Table 2. ΔJR−FL protein has higher affinity to sCD4 than JR−FL protein (by about 7-fold). From the relative affinities measured, the ΔJR−FL protein would be somewhat more saturated than JR−FL protein at the experimental mixture ratios used in 17b binding experiments ([JR−FL gp120]:[sCD4] = 1:15; [ΔJR−FL gp120]:[sCD4] = 1:25). Nonetheless, the faster on rate of ΔJR−FL protein vs JR−FL protein to immobilized 17b Fab when sCD4 is present persists even at the highest concentrations used, where saturation differences between the two gp120 forms are small (98.8% for JR−FL vs 99.8% for ΔJR−FL). Hence, the faster on rates of ΔJR−FL protein binding to 17b in the presence of sCD4 can be surmised to reflect the structural

Table 1: Summary of Kinetic Constants from Global Analysis of the Biosensor Binding of HIV-1 Env Glycoprotein (JR−FL and ΔJR−FL Protein) to Immobilized Antibody (17b Fab)[b]

gp120		k_{on} (10^4 M^{-1} s^{-1})	k_{off} (10^{-4} s^{-1})	K_d (10^{-9} M)
JR−FL	−sCD4	2.7 ± 0.1 (2.0)	0.76 ± 0.1 (0.9)	2.8 ± 0.4 (4.5)
JR−FL	+sCD4	59 ± 2 (53)	0.59 ± 0.1[c] (0.57[c])	0.1 ± 0.3[c] (0.11[c])
ΔJR−FL	−sCD4	11.3 ± 0.2 (10)	1.1 ± 0.2 (1.7)	0.93 ± 0.4 (1.7)
ΔJR−FL	+sCD4	186 ± 3 (180)	0.76 ± 0.2[c] (0.87[c])	0.041 ± 0.02[c] (0.048)[c]

[a] Linear transformation analysis results are shown in parentheses. [b] Values are the average of the data from three different surface densities. K_d values are calculated from k_{off}/k_{on}. [c] These values are considered apparent due to the possibility that the off rates are affected not only by dissociation of CD4−gp120 complex from 17b but also by dissociation of CD4 alone from gp120−17b complex (see Discussion).

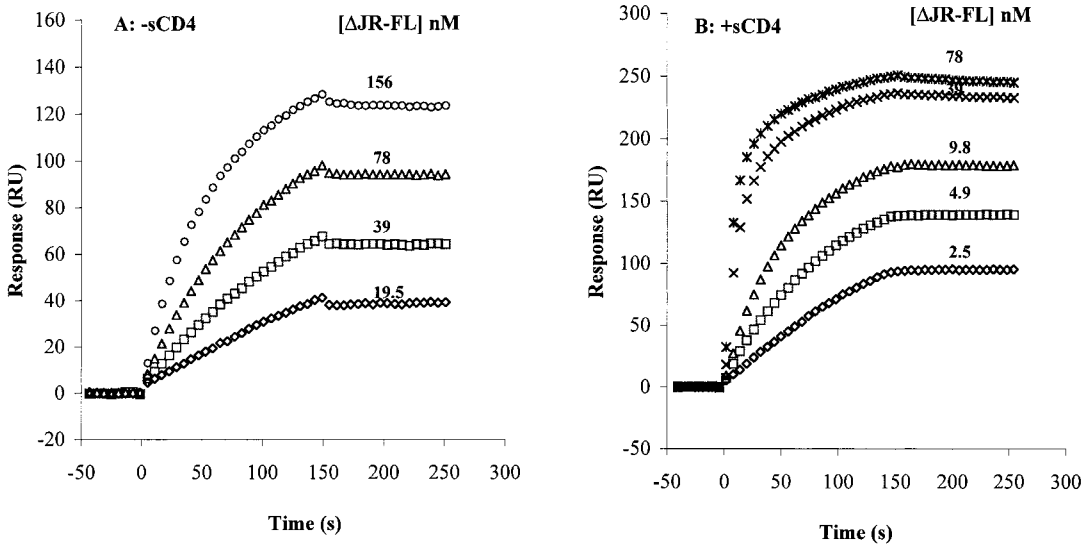

FIGURE 5: Sensorgram overlays for ΔJR−FL protein binding to immobilized 17b Fab surface. Surface density, 620 RU; buffer, 10 mM phosphate, pH 7.4, 150 mM NaCl, and 0.005% Tween; flow rate, 60 μL/min. ΔJR−FL protein concentrations are shown at the right of each sensorgram. (A) In the absence of sCD4. (B) In the presence of sCD4; the sCD4 concentration in each mixture is 25 times that of each ΔJR−FL concentration.

difference of the gp120−sCD4 complexes, not simply the influence of CD4 saturation.

Biosensor-Detected 17b Binding Effects in JR−FL Induced by Charybdotoxin-Based CD4 Mimetic. Drakopoulou et al. (*49*) recently described a 33-amino acid peptide derived from charybdotoxin that was designed to be a mimetic of the gp120 binding site on CD4. This peptide was found by ELISA analysis to inhibit gp120 binding to CD4 with an IC_{50} of 20 μM, which was 2.5×10^4-fold greater than that observed with the CD4 protein. Using the same scaffold in conjunction with the recently reported cocrystal structure of the CD4−gp120 complex (*21*), we designed a new charybdotoxin sequence and used biosensor analysis to investigate its mimetic characteristics, including induction of increased 17b affinity. The native charybdotoxin molecule possesses a well-defined folded structure with a small antiparallel β-sheet connected to a short α-helix by a β-turn (*48, 50*). The whole molecule is folded into this α/β structure motif by three disulfide bonds. This structure motif is well conserved in all known scorpion toxins and tolerates a large number of non-Cys amino acid mutations in the molecule without loss of folding (*50, 51*).

The charybdotoxin analogue molecule we designed, TXM1, is

10 20 30
NH_2-**G**CTTSKECWSVCQRLHNTSRG**G**C**QGSF**C**T**C**GP**-OH

The underlined residues in this sequence are noncharybdotoxin sequence elements that were incorporated to mimic structural features of CD4, in particular near the Phe 43 binding loop region. The TXM1 sequence is identical to the CD4 mimetic of Drakopoulou et al. (*49*) except in two positions, (A) Arg in place of Lys at residue 20 and (B) Gly in place of Val at residue 1. We preserved Arg20 of charybdotoxin since the corresponding Lys in CD4 does not appear to be involved in binding to gp120 (*21*). The Gly at residue 1 places an α-amino group relative to the Phe 27 in a position which is similar to that of the critical Arg 59 guanidino group relative to Phe 43 in the CD4−gp120 cocrystal structure (*21*). Also, the Gly at position 1 avoids possible steric hindrance that could occur with larger side chain residues and the complexity of two positively charged groups that would occur with an Arg itself at this position. The energy-minimized structure of TXM1 and its comparison with CD4 crystal structure are shown in Figure 8.

The effect of TXM1 and TXM0, in which residues 26 and 27 are SF and FS, respectively (see sequences in Experimental Procedures and Figure 8 right for the side-chain position of Phe 26) on gp120 binding to 17b Fab was tested with the same surface configuration as described above for sCD4. The sensorgram overlays shown in Figure 9 were collected on a 17b Fab surface with 1600 RU surface density. The molar concentration ratio between JR−FL and TXM1 or TXM0 was 1:50. There was no significant effect of TXM1 on the apparent off rate. However, there was an increasing

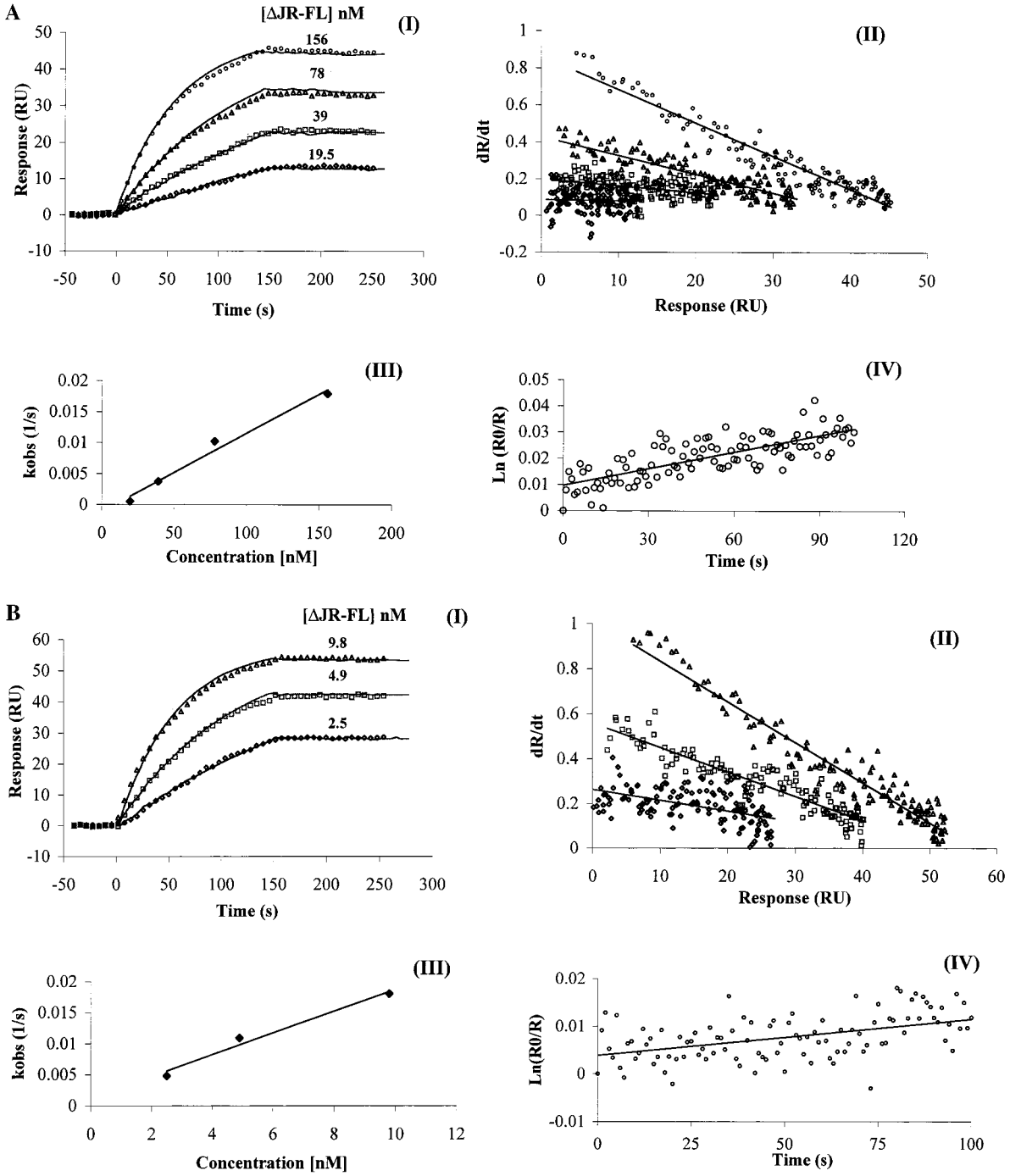

FIGURE 6: (A) Curve-fitting analysis of ΔJR−FL gp120 protein binding to immobilized 17b (150 RU) Fab in the absence of sCD4. (I) Global analysis: the symbols are the experimental data, and the lines are the best fit to a 1:1 binding model. (II−IV) Linear transformation analyses: (II) dR/dt vs R plot; (III) k_{obs} vs concentration plot, where the slope of the line is k_{on}; (IV) ln (R_0/R) vs time plot of the 156 nM curve in plot I, where R_0 is the starting point of dissociation and the slope of the line gives k_{off}. (B) Curve-fitting analysis of ΔJR−FL gp120 protein binding to immobilized 17b (150 RU) Fab in the presence of sCD4. Plots I−III are as in panel A. In plot IV, the ln (R_0/R) vs time plot is for the 9.8 nM curve in plot I, where R_0 is the starting point of dissociation and the slope of the line gives k_{off}.

effect on the on rate, which was smaller than the effect of sCD4. Curve-fitting analysis by global minimization with a 1:1 binding model revealed a 2.5-fold increase in on rate when TXM1 was present (Table 3). Importantly, no effect on binding kinetics was observed when TXM0 was tested in place of TXM1 (Figure 9B).

Competition Assay of TXM1 Binding to the CD4 Binding Site in gp120. The ability of TXM1 to bind to gp120 was tested by competition of gp120 binding to sensor-immobilized sCD4. The surface density of sCD4 was kept low (150 RU), since the affinity of TXM1 to gp120 is much weaker than that of sCD4. Slow flow rate (4 μL/min) and longer association time (25 min) were employed to compare the steady-state binding. The sensorgram overlays are shown in Figure 10. Both on-rate constants (k_{on} in Table 3) and maximum binding at steady state (Figure 10) were reduced when TXM1 was present. Both of these reduced parameters of the sensor kinetics argue that TXM1 competes with sCD4 for gp120 binding and likely binds at the CD4 binding site in the latter.

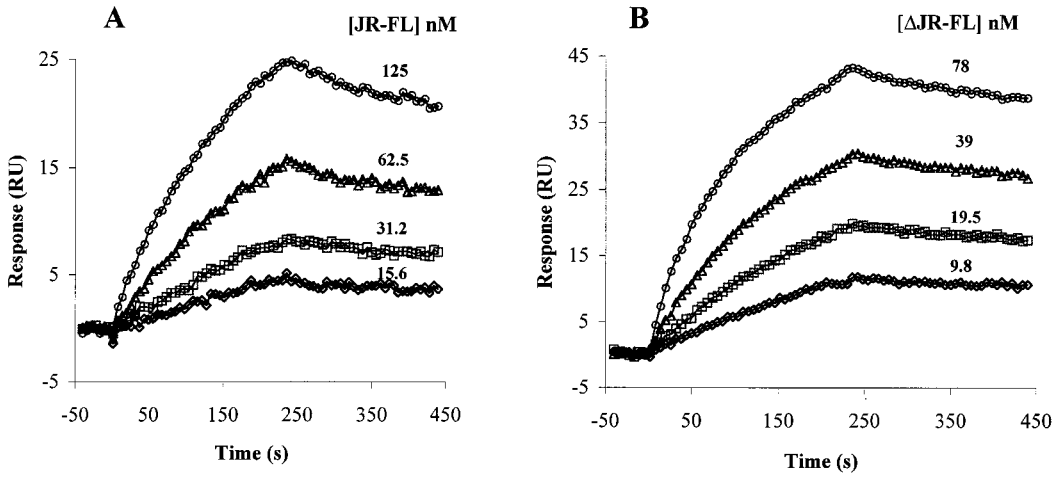

FIGURE 7: Sensorgram overlays for gp120 proteins binding to immobilized sCD4 (200 RU surface). Buffer, 10 mM phosphate, pH 7.4, 150 mM NaCl, and 0.005% Tween; flow rate, 40 μL/min. (A) Full-length JR−FL gp120 protein; (B) Mutant ΔJR−FL. JR−FL and ΔJR−FL protein concentrations are indicated at the right of each graph.

Table 2: Summary of Kinetic Constants for the Interaction of HIV-1 Env Glycoprotein (JR−FL and ΔJR−FL) to Sensor-Immobilized sCD4[a]

gp120	k_{on} (10^4 M^{-1} s^{-1})	k_{off} (10^{-4} s^{-1})	K_d (10^{-9} M)
JR−FL	3.5 ± 0.1 (4.5)	7.7 ± 0.8 (7.5)	22 ± 0.4 (17)
ΔJR−FL	12 ± 0.1 (10)	3.9 ± 0.5 (4.5)	3.2 ± 0.6 (4.5)

[a] Kinetic constants were obtained by global analysis (and linear transformation analysis in parentheses). The values were the average of data from two different surface densities of immobilized sCD4. K_d values are calculated from k_{off}/k_{on}.

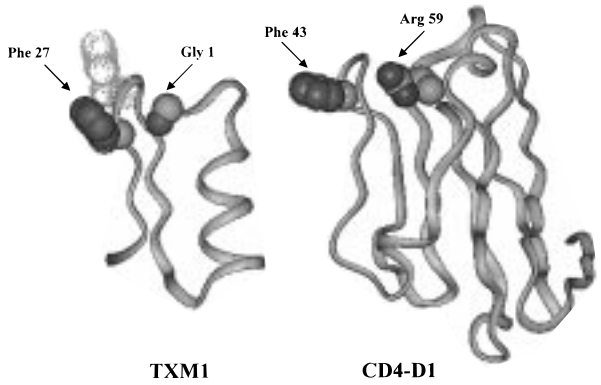

FIGURE 8: Structure comparison of TXM1 and CD4. (Right) TXM1. The structure shown was obtained by homology modeling to the NMR structure of charybdotoxin (PDB code: 2crd) followed by energy minimization using InsightII 97.0 (Molecular Simulations Inc., 1997). (Left) D1 portion of CD4 crystal structure (*52*). The key residues, Phe27 side chain and Gly1 amino terminus in TXM1 and Phe43 and Arg59 side chains in CD4, are labeled. The dotted van der Waals surface in the figure on the right represents the Phe26 side-chain position in TXM0.

DISCUSSION

The cooperative effect of CD4 binding on the efficacy of HIV-1 env to bind chemokine receptor and to trigger ensuing virus−cell fusion makes it important to determine the structural and mechanistic features of binding of these two gp120 protein ligands that lead to cooperativity. However, chemokine receptors are integral seven-transmembrane segment receptors, and hence molecular and biophysical assays are difficult to perform with this cell-surface component. To circumvent this limitation in investigating the cooperative events in the gp120−CD4−CCR5 interaction, we have focused on incorporating a CCR5 surrogate, antibody 17b, into interaction studies. The neutralizing human antibody 17b recognizes a discontinuous conserved epitope in gp120 that overlaps with the chemokine receptor binding site (*26*, *29*, *30*, *39*, *40*). The 17b antibody thus provides a probe to follow ligand-induced conformational changes in gp120 and their effect on the binding of gp120 to CCR5. In the current study, we developed a three-component CD4−gp120−17b sensor configuration to visualize CD4-induced conformational rearrangements in gp120. We also showed that a CD4 mimetic miniprotein, which contains a limited number of structural elements of CD4 transplanted into its conformational scaffold, is able to trigger a CD4-like conformational isomerization of gp120.

The biosensor assay established in this work incorporated conditions such as flow rate and 17b Fab surface density to maximize the likelihood that the binding interaction was under kinetic control and to minimize artifacts such as mass transport and nonspecific binding to the sensor surface. Using this assay, we observed a much greater 17b binding on rate and overall affinity for JR−FL gp120 protein when sCD4 is prebound. This provides a straightforward indication of transition in gp120 from a low-reactivity to high-reactivity form. This result is consistent with earlier findings that the 17b-recognizing epitope on gp120 is more exposed upon CD4 binding, as judged from data on efficiency of precipitation of the envelope glycoprotein by 17b antibody and ELISA assay of 17b antibody binding to plate-coated envelope glycoproteins (*30*). Since the 17b epitope is near the CCR5-binding domain, we conclude that higher affinity 17b binding (mainly faster on rate) implies a higher affinity CCR5 binding of gp120. The three-component biosensor assay is a potentially useful vehicle to determine structure−function relationships in the CD4 and gp120 components that facilitate CCR5 binding and consequent virus cell entry.

In the absence of sCD4, the loop-deleted gp120 mutant ΔJR−FL protein has a faster association rate and higher affinity for 17b Fab than full-length gp120, JR−FL protein. This is consistent with the view that the 17b binding epitope in ΔJR−FL protein, in which the V1/V2 loops are deleted, is more accessible than in full-length gp120. However, in

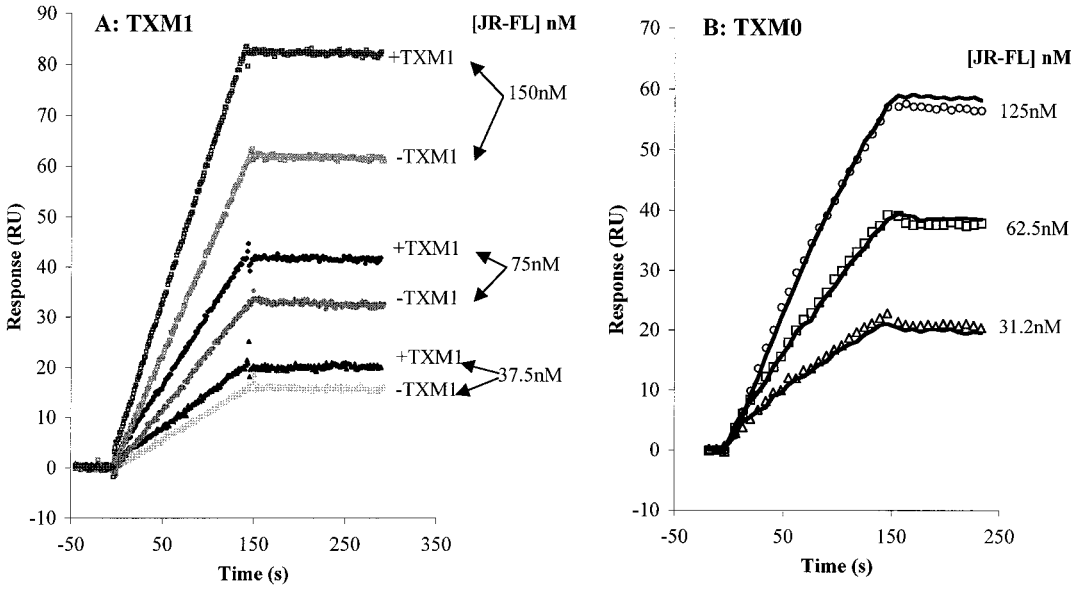

FIGURE 9: Sensorgram overlays for the JR−FL protein binding to immobilized 17b Fab in the absence and presence of TXM1 (A) and TXM0 (B). Surface density, 1600 RU; buffer, 10 mM phosphate, pH 7.4, 300 mM NaCl, and 0.005% Tween. JR−FL protein concentrations are shown at the right of each sensorgram. Flow rate: 30 μL/min. The concentration of TXM1 and TXM0 in each mixture is 50 times that of each JR−FL concentration. In panel B, the curves with symbols are data in the presence of TXM0, and the curves with lines are data in the absence of TXM0.

Table 3: Comparison of On Rates of JR−FL gp120 Glycoprotein Binding to Immobilized 17b Fab and sCD4 in the Absence and Presence of TXM1[a]

	17b surface[b] k_{on} (10^3 M^{-1} s^{-1})	sCD4 surface[c] k_{on} (10^4 M^{-1} s^{-}1)
−TXM1	1.7	3.0
+TXM1	4.3	2.5

[a] Data were obtained by global analysis. [b] From Figure 9A. [c] From Figure 10.

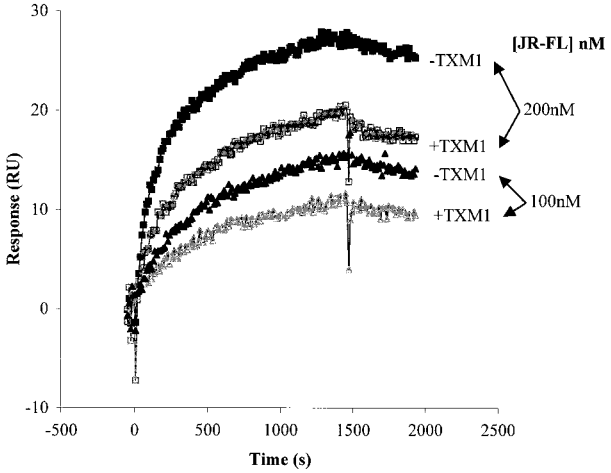

FIGURE 10: Sensorgram overlays for JR−FL gp120 protein binding to immobilized sCD4 surface in the absence and presence of TXM1. Surface density, 150 RU; buffer, 10 mM sodium phosphate, pH 7.4, 300 mM NaCl, and 0.005% Tween. JR−FL gp120 concentrations are shown at the right of each sensorgram. Flow rate: 4 μL/min. The concentration of TXM1 in each mixture is 20 times that of each JR−FL gp120 protein concentration.

the presence of sCD4, we also observed a large affinity increase of ΔJR−FL protein binding to 17b compared to that in the absence of sCD4, similar to what we found with full-length gp120, JR−FL protein. This suggests that the conformational transition in gp120 that effects higher 17b affinity involves conformational changes beyond the movement of the V1/V2 loops that unmask the CD4i binding site in gp120 when sCD4 binds. CD4 binding also appears to introduce or stabilize a structural rearrangement in gp120 core structure that leads to a higher affinity form of the 17b binding site. A large conformational rearrangement of the gp120 core is consistent with the finding from microcalorimetry measurements in which an unusually large ΔH and compensating $T\Delta S$ values were observed upon CD4 binding to gp120 in solution (M. L. Doyle, personal communication). While CD4-induced conformational isomerization of the V1/V2 loops can be surmised to occur while gp120 is assembled in the viral envelope, the possibility that core rearrangement also occurs in the assembled state is much less certain.

Interestingly, comparison of the kinetic constants of JR−FL protein to those of ΔJR−FL protein in the presence of sCD4 reveals that ΔJR−FL protein has faster association and dissociation rate than JR−FL protein even though their K_d values are similar. One explanation is that while the 17b binding site is more accessible in the truncated derivative, truncation has eliminated structural elements that stabilize the 17b−gp120 complex. Such stabilizing structural elements require further investigation, and indeed the three-component biosensor asssay could be useful in such investigation. Nonetheless, an important caveat in the above is the possibility that the faster off rate observed with ΔJR−FL protein is due to dissociation not of the deleted envelope protein−CD4 complex but of CD4 itself, or some mixture of the two dissociation events. Indeed, the dissociation rates of env protein−CD4 complexes from 17b must be treated with caution due to the possible contribution of both CD4-alone and env−CD4 complex dissociation. The fact that the dissociation processes in both CD4-present and CD4-absent sensorgrams are similarly fitted to a simple 1:1 bimolecular interaction model argues in favor of the notion that the dissociation process is not affected significantly by CD4-

alone dissociation. Nonetheless, it cannot be ruled out that the biosensor assay may not be sensitive enough over the whole time range to detect the mixture of dissociation processes.

Since the 17b binding site on gp120 overlaps with chemokine coreceptor CCR5 binding site, the three-component gp120−CD4−17b biosensor assay provides a potentially useful tool to investigate how CD4 binding induces conformational isomerization to promote viral docking and cell fusion. This assay also provides a method to assess the effect of CD4 mimetics on gp120 conformational change. Hence the assay may be a useful guide for the design of CD4 mimetic antagonists that, for example, do not cause conformation change and hence could trap HIV-1 env in a fusion-deficient state.

The CD4 miniprotein mimetic TXM1 studied here is based on the scorpion charybdotoxin, which has a loop structure similar to the loop structure in the Phe 43 region of CD4 (*21*, *49*). Three disulfide bonds are key elements that stabilize folding of the molecule into the common tertiary structure found in the scorpion toxin family. Mutations of non-Cys residues are well tolerated without changing this overall tertiary fold (*50*, *51*). A set of residues in TXM1 sequence (see Results) were transplanted from native CD4 regions in or near the Phe 43/Arg 59 motif.

In the gp120−17b binding assay, the presence of TXM1 increased the association rate by 2.5-fold while leading to no apparent change in the observed off rate. The mimetic is sufficiently small that its dissociation from a 17b−env complex is unlikely to lead to a significant decrease in response in the dissociation phase, and hence the off rates measured in the presence of miniprotein are likely reflective mainly of env dissociation. Consequently, the miniprotein mimetic TXM1 can be assumed to enhance the observed env affinity to 17b Fab by about 2.5-fold. The on-rate enhancement of TXM1 argues that this molecule induces a CD4-like conformational isomerization in the gp120 molecule that leads to greater exposure of the 17b binding site. The ability of TXM1 to compete with the gp120−CD4 binding confirms that the miniprotein binds to a similar site on gp120 as CD4. Both the 17b binding enhancement and CD4 binding inhibition effects of TXM1 on JR−FL env were only observed to partial completion (vs the effect by CD4), in large part due to the apparently lower affinity of TXM1 vs CD4. An estimate of affinity from the response of bound signal to TXM1 concentration in Figure 9A gives a value of 20 μM, which is comparable to the IC_{50} value for inhibition of gp120 binding to CD4 by the related mimetic described by Drakopoulou et al. (*49*). Increasing TXM1 miniprotein concentrations to greater than 5 μM in the current work led to apparent increases in both 17b binding enhancement and CD4 binding inhibition effects seen with the biosensor assays. However, quantitation of the resulting data was severely impeded by optical artifacts that distorted the sensorgrams. Nevertheless, TXM1 can serve as a starting miniprotein sequence for the development of higher affinity CD4 mimetics, for example around the α-amino group and Phe 27. In addition, the 17b−gp120−CD4 three-component biosensor assay can serve as a useful means to identify the conformational isomerization effects of these mimetic molecules.

ACKNOWLEDGMENT

We thank Mr. Andrew Prantner and Dr. Stanley Opella for use of the PerSeptive peptide synthesizer in his laboratory in the Chemistry Department at UPenn. We thank Drs. James Samanen, Catherine Peishoff, and Michael Doyle (Smith-Kline Beecham) for helpful discussion during this work. We also thank Dr. Claudio Vita (CEA, Saclay, France) for making results of his work available to us in advance of their publication in *Letters in Peptide Science* (*49*).

REFERENCES

1. Gallo, R. C., Salahuddin, S. Z., Popovic, M., Shearer, G. M., Kaplan, M., Haynes, B. F., Palker, T. J., Redfield, R., Oleske, J., Safai, B., et al. (1984) *Science 224*, 500−3.
2. Barre-Sinoussi, F., Chermann, J. C., Rey, F., Nugeyre, M. T., Chamaret, S., Gruest, J., Dauguet, C., Axler-Blin, C., Vezinet-Brun, F., Rouzioux, C., Rozenbaum, W., and Montagnier, L. (1983) *Science 220*, 868−71.
3. Allan, J. S., Coligan, J. E., Barin, F., McLane, M. F., Sodroski, J. G., Rosen, C. A., Haseltine, W. A., Lee, T. H., and Essex, M. (1985) *Science 228*, 1091−4.
4. Earl, P. L., Moss, B., and Doms, R. W. (1991) *J. Virol. 65*, 2047−55.
5. Robey, W. G., Safai, B., Oroszlan, S., Arthur, L. O., Gonda, M. A., Gallo, R. C., and Fischinger, P. J. (1985) *Science 228*, 593−5.
6. Dalgleish, A. G., Beverley, P. C., Clapham, P. R., Crawford, D. H., Greaves, M. F., and Weiss, R. A. (1984) *Nature 312*, 763−7.
7. Klatzmann, D., Champagne, E., Chamaret, S., Gruest, J., Guetard, D., Hercend, T., Gluckman, J. C., and Montagnier, L. (1984) *Nature 312*, 767−8.
8. Maddon, P. J., Dalgleish, A. G., McDougal, J. S., Clapham, P. R., Weiss, R. A., and Axel, R. (1986) *Cell 47*, 333−48.
9. Sattentau, Q. J., and Moore, J. P. (1991) *J. Exp. Med. 174*, 407−15.
10. Sattentau, Q. J., Moore, J. P., Vignaux, F., Traincard, F., and Poignard, P. (1993) *J. Virol. 67*, 7383−93.
11. Alkhatib, G., Combadiere, C., Broder, C. C., Feng, Y., Kennedy, P. E., Murphy, P. M., and Berger, E. A. (1996) *Science 272*, 1955−8.
12. Choe, H., Farzan, M., Sun, Y., Sullivan, N., Rollins, B., Ponath, P. D., Wu, L., Mackay, C. R., LaRosa, G., Newman, W., Gerard, N., Gerard, C., and Sodroski, J. (1996) *Cell 85*, 1135−48.
13. Deng, H., Liu, R., Ellmeier, W., Choe, S., Unutmaz, D., Burkhart, M., Di Marzio, P., Marmon, S., Sutton, R. E., Hill, C. M., Davis, C. B., Peiper, S. C., Schall, T. J., Littman, D. R., and Landau, N. R. (1996) *Nature 381*, 661−6.
14. Feng, Y., Broder, C. C., Kennedy, P. E., and Berger, E. A. (1996) *Science 272*, 872−7.
15. Doranz, B. J., Rucker, J., Yi, Y., Smyth, R. J., Samson, M., Peiper, S. C., Parmentier, M., Collman, R. G., and Doms, R. W. (1996) *Cell 85*, 1149−58.
16. Dragic, T., Litwin, V., Allaway, G. P., Martin, S. R., Huang, Y., Nagashima, K. A., Cayanan, C., Maddon, P. J., Koup, R. A., Moore, J. P., and Paxton, W. A. (1996) *Nature 381*, 667−73.
17. Starcich, B. R., Hahn, B. H., Shaw, G. M., McNeely, P. D., Modrow, S., Wolf, H., Parks, E. S., Parks, W. P., Josephs, S. F., Gallo, R. C., et al. (1986) *Cell 45*, 637−48.
18. Wiley, C. A., Schrier, R. D., Nelson, J. A., Lampert, P. W., and Oldstone, M. B. (1986) *Proc. Natl. Acad. Sci. U.S.A. 83*, 7089−93.
19. Thali, M., Moore, J. P., Furman, C., Charles, M., Ho, D. D., Robinson, J., and Sodroski, J. (1993) *J. Virol. 67*, 3978−88.
20. Wyatt, R., Kwong, P. D., Desjardins, E., Sweet, R. W., Robinson, J., Hendrickson, W. A., and Sodroski, J. G. (1998) *Nature 393*, 705−11.

21. Kwong, P. D., Wyatt, R., Robinson, J., Sweet, R. W., Sodroski, J., and Hendrickson, W. A. (1998) *Nature 393*, 648−59.
22. Wyatt, R., Desjardin, E., Olshevsky, U., Nixon, C., Binley, J., Olshevsky, V., and Sodroski, J. (1997) *J. Virol. 71*, 9722−31.
23. Leonard, C. K., Spellman, M. W., Riddle, L., Harris, R. J., Thomas, J. N., and Gregory, T. J. (1990) *J. Biol. Chem. 265*, 10373−82.
24. Ho, D. D., McKeating, J. A., Li, X. L., Moudgil, T., Daar, E. S., Sun, N. C., and Robinson, J. E. (1991) *J. Virol. 65*, 489−93.
25. Posner, M. R., Hideshima, T., Cannon, T., Mukherjee, M., Mayer, K. H., and Byrn, R. A. (1991) *J. Immunol. 146*, 4325−32.
26. Rizzuto, C. D., Wyatt, R., Hernandez-Ramos, N., Sun, Y., Kwong, P. D., Hendrickson, W. A., and Sodroski, J. (1998) *Science 280*, 1949−53.
27. Thali, M., Furman, C., Ho, D. D., Robinson, J., Tilley, S., Pinter, A., and Sodroski, J. (1992) *J. Virol. 66*, 5635−41.
28. Trkola, A., Purtscher, M., Muster, T., Ballaun, C., Buchacher, A., Sullivan, N., Srinivasan, K., Sodroski, J., Moore, J. P., and Katinger, H. (1996) *J. Virol. 70*, 1100−8.
29. Trkola, A., Dragic, T., Arthos, J., Binley, J. M., Olson, W. C., Allaway, G. P., Cheng-Mayer, C., Robinson, J., Maddon, P. J., and Moore, J. P. (1996) *Nature 384*, 184−7.
30. Wyatt, R., Moore, J., Accola, M., Desjardin, E., Robinson, J., and Sodroski, J. (1995) *J. Virol. 69*, 5723−33.
31. Allan, J. S., Strauss, J., and Buck, D. W. (1990) *Science 247*, 1084−8.
32. Allan, J. S. (1991) *Science 252*, 1322−3.
33. Allan, J. S., Whitehead, E. M., Strout, K., Short, M., Kanda, P., Hart, T. K., and Bugelski, P. J. (1992) *AIDS Res. Hum. Retroviruses 8*, 2011−20.
34. Denisova, G., Raviv, D., Mondor, I., Sattentau, Q. J., and Gershoni, J. M. (1997) *J. Immunol. 158*, 1157−64.
35. Moore, J. P., McKeating, J. A., Weiss, R. A., and Sattentau, Q. J. (1990) *Science 250*, 1139−42.
36. Sattentau, Q. J., Zolla-Pazner, S., and Poignard, P. (1995) *Virology 206*, 713−7.
37. Sullivan, N., Sun, Y., Sattentau, Q., Thali, M., Wu, D., Denisova, G., Gershoni, J., Robinson, J., Moore, J., and Sodroski, J. (1998) *J. Virol. 72*, 4694−703.
38. Willey, R. L., Martin, M. A., and Peden, K. W. (1994) *J. Virol. 68*, 1029−39.
39. Wu, L., Gerard, N. P., Wyatt, R., Choe, H., Parolin, C., Ruffing, N., Borsetti, A., Cardoso, A. A., Desjardin, E., Newman, W., Gerard, C., and Sodroski, J. (1996) *Nature 384*, 179−83.
40. Moore, J. P., and Sodroski, J. (1996) *J. Virol. 70*, 1863−72.
41. Binley, J. M., Wyatt, R., Desjardins, E., Kwong, P. D., Hendrickson, W., Moore, J. P., and Sodroski, J. (1998) *AIDS Res. Hum. Retroviruses 14*, 191−8.
42. Culp, J. S., Johansen, H., Hellmig, B., Beck, J., Matthews, T. J., Delers, A., and Rosenberg, M. (1991) *Bio/Technology 9*, 173−7.
43. Arthos, J., Deen, K. C., Chaikin, M. A., Fornwald, J. A., Sathe, G., Sattentau, Q. J., Clapham, P. R., Weiss, R. A., McDougal, J. S., Pietropaolo, C., et al. (1989) *Cell 57*, 469−81.
44. Ryu, S. E., Kwong, P. D., Truneh, A., Porter, T. G., Arthos, J., Rosenberg, M., Dai, X. P., Xuong, N. H., Axel, R., Sweet, R. W., et al. (1990) *Nature 348*, 419−26.
45. Fields, C. G., and Fields, G. B. (1994) *Methods Mol. Biol. 35*, 29−40.
46. Pennington, M. W. (1994) *Methods Mol. Biol. 35*, 41−62.
47. Andreu, D., Albericio, F., Sole, N. A., Munson, M. C., Ferrer, M., and Barany, G. (1994) *Methods Mol. Biol. 35*, 91−169.
48. Vita, C., Bontems, F., Bouet, F., Tauc, M., Poujeol, P., Vatanpour, H., Harvey, A. L., Menez, A., and Toma, F. (1993) *Eur. J. Biochem. 217*, 157−69.
49. Drakopoulou, E., Vizzavona, J., and Vita, C. (1998) *Lett. Pept. Sci. 5*, 241−245.
50. Vita, C., Vizzavona, J., Drakopoulou, E., Zinn-Justin, S., Gilquin, B., and Menez, A. (1998) *Biopolymers 47*, 93−100.
51. Bontems, F., Roumestand, C., Gilquin, B., Menez, A., and Toma, F. (1991) *Science 254*, 1521−3.

BI990654O